Extraction of impervious surface in Hai Basin using remote sensing

WANG Hao, WU Bingfang, LI Xiaosong, LU Shanlong

Institute of Remote Sensing Applications, Chinese Academy of Science, Beijing 100101*, China*

Abstract: Impervious surface coverage in a region is not only an indicator of the degree of urbanization but also a major indicator of environmental quality. Most of the existing methods of extracting impervious surface based on remote sensing concentrate on an urban scale, but the rapid and accurate methods of extracting impervious surfaces in a basin scale are nearly nonexistent in China and abroad. In this study, we used Landsat images acquired in same season covering the entire Hai Basin as data source, and generated a mask for removing the non-impervious surfaces using a land-use data set of roads, and urban, rural, and industrial land. Then, by selecting bright and dark vegetation endmember, high albedo and low albedo impervious surface endmember, and dry and wet soil endmember, we applied a Multiple Endmember Spectral Mixture Analysis (MESMA) model to extract impervious surfaces in the basin scale. The accuracy assessment results showed high accuracy, in that the mean relative error (MRE) and correlation coefficient (R) of all samples were 12.1% and 0.83, respectively, which indicated that the method of extracting impervious surfaces in a basin scale was feasible.

Key words: impervious surface, basin scale spectral mixture analysis, remote sensing, Hai Basin

CLC number: TP75/TP79 **Document code:** A

Citation format: Wang H, Wu B F, Li X S and Lu S L. 2011. Extraction of impervious surface in Hai Basin using remote sensing. *Journal of Remote Sensing*, **15**(2): 388–400

1 INTRODUCTION

Impervious surfaces are anthropogenic features through which water cannot infiltrate into the soil, such as rooftops, roads, driveways, sidewalks, and parking lots, among others (Arnold & Gibbons, 1996). Impervious surface coverage is the percentage of impervious surface in an area as large as a drainage basin or as small as an area which a pixel stands for. With the rapid development of the social economy, the degree of urbanization has become higher and higher, which leads to an increase in impervious surfaces.

In an urban scale, impervious surface coverage is an indicator of the degree of urbanization, as well as a term that is widely used in urban related studies (Wu & Murray, 2005; Lu, *et al*., 2006), such as residential population estimation, land-use and land-cover mapping (Madhavan, *et al*., 2001; Phinn, *et al*., 2002; Lu & Weng, 2006; Pu, *et al*., 2008), and urban land-use planning (Brabec, *et al*., 2002). In addition, impervious surfaces absorb a large amount of short-wave solar radiation, which then heats the urban canopy layer and boundary layer in the form of long-wave radiation and alters the sensible and latent heat flux (Oke, 1987; Yuan & Bauer, 2006). This has an overall effect on the climate of city and urban agglomeration.

In a basin scale, rainfall in impervious surface areas infiltrates into the soil with difficulty, so soil water and ground water are found in insufficient supplies; correspondingly, more water from rainfall generates surface runoff and is accumulated in rivers, which increases the storm flow and flooding frequency (Brun & Band, 2000; Weng, 2001). The increase in impervious surfaces and runoff directly impacts the transport of non-point source pollutants, including pathogens, nutrients, toxic contaminants, and sediment (Hurd & Civco, 2004), which has a profound negative impact on water quality of lakes, streams, and other aquatic environments (Zug, *et al*., 1999; Brabec, *et al*., 2002; Gillies, *et al*., 2003). Generally, most stream health indicators decline when impervious surface coverage of a basin exceeds 10%. In summary, the impervious surface is an important land surface characteristic of the hydrological cycle and water resource assessment in a basin.

The methods of extracting impervious surfaces based on remote sensing mainly include pixel-based classification (Hodgson, *et al*., 2003; Dougherty, *et al*., 2004; Jennings, *et al*., 2004) and sub-pixel extraction (Civco & Hurd, 1997; Gillies *et al*., 2003; Bauer, *et al*., 2004; Yang X, 2006; Murray, 2003; Yang, *et al*., 2003a, b; Wu, 2004; Jantz, *et al*., 2005; Lu & Weng, 2006; Xian, 2007). In traditional impervious surface extraction, pixel-based classification long has been the dominant method. The impervious surface is considered to be a land type and can be captured through a variety of supervised and unsupervised classifications. Due to the limits of image resolution, impervious surface and other land types often are mixed in a pixel. In order to solve the mixed pixel problem, scientists

Received: 2010-06-02; **Accepted:** 2010-08-02

Foundation: The Knowledge Innovation Program of the Chinese Academy of Sciences (No. KZCX1-YW-08-03); The National Key Technology R&D Program (No. 2006BAJ11B09).

First author biography: WANG Hao (1985—), male, PHD student, Institute of Remote Sensing of Applications of Sciences. He majors in extraction of land surface parameters and remote sensing estimation of water resources. E-mail: wanghao@irsa.ac.cn

Responding author: WU Bingfang, E-mail:wubf@irsa.ac.cn

have developed a sub-pixel level of impervious surface extraction, and the extracting methods include use of a multiple regression model (Gillies, *et al*., 2003; Bauer, *et al*., 2004; Yang X, 2006), spectral mixture analysis (Wu & Murray, 2003; Wu, 2004; Lu & Weng, 2006), an artificial neural network (Civco & Hurd, 1997), and a classification and regression tree (Yang X, *et al*., 2003a, b; Jantz, *et al*., 2005; Xian, 2007), among others. Due to the development of sub-pixel extraction, one single landtype was replaced by a continuous impervious surface coverage to represent the composition of a pixel, and as a result, the extraction of impervious surfaces reaches a quantitative level.

Although many methods of extracting impervious surfaces have emerged in China and abroad, almost all of the studies are limited to the urban scale, and methods for a fast and accurate extraction of impervious surfaces in a basin scale have not been established. However, many water resource exploitation and utilization, river management and planning, and water cycle process research are conducted in a basin scale. The basin is the basic unit of hydrological cycle study because it is closed. Therefore, extraction of impervious surface distribution in a whole basin using remote sensing has significant meaning for hydrological cycle and water resource assessment.

This paper aims to explore an impervious surface extraction method in a basin scale and to map the impervious surface distribution of the entire Hai Basin, so it can serve for water cycle research in a basin scale. In this study, we chose the Hai Basin as our study area and chose Landsat ETM+ satellite images and ancillary land use as our data source. By selecting bright and dark vegetation endmember, high albedo and low albedo impervious surface endmember, and dry and wet soil endmember, we applied the MESMA model to extract impervious surface coverage. Finally, through NDVI threshold selection and origin impervious surface coverage normalization, we obtained the exact impervious surface distribution of the entire Hai Basin.

2 DATA AND METHODOLOGY

2.1 Data and preprocessing

(1) Landsat ETM+

Twenty scene Landsat images cover the entire Hai Basin, and the time of acquisition was from July 1, 1997 to May 22, 2002. Each scene was taken in late spring to early fall, which was during the vegetation growing season.

The Landsat data were downloaded from the U.S. Geological Survey (USGS) Web site, and they were geometrically corrected so no re-registrations were needed. Because no clouds or few clouds were found in each scene, no atmospheric correction was performed.

(2) Land use

The land use data for this study were from the Chinese Academy of Science Bureau of Resources and Environmental, and the original images used for mapping the land use data are the same as those referred to in the last paragraph. Because impervious surface extraction focuses on the impervious surface in urban areas, agricultural areas and forest-grass areas, where impervious surfaces are few, were removed.

The urban residential land (code 71), rural residential land (code 72), industrial area (code 61), road (code 101), and rail (code 102) land types in the land use data sets were combined to generate a mask, and the mask was used to remove the other land types to increase the precision and accuracy of impervious surface coverage extraction.

(3) High-resolution image

The high-resolution image was an aerial orthophotograph taken in August, 2000 with its spatial resolution set to 1 m. We used this orthophotograph to evaluate the accuracy of extracted impervious surfaces.

Due to the high resolution of the images, the impervious surfaces determined through classification were deemed to be actual impervious surfaces. Therefore, we were able to use the classification results to evaluate the accuracy of the remote sensing extraction results.

2.2 Determination of model

The linear spectral mixture model depicts the reflectance of a band in each pixel as a linear summation of the reflectance of each endmember multiplied its weight (Zhao, 2003). The endmember is pure land cover type, and the weight is determined by surface fraction of each endmember. The model is based on the following three hypotheses: (1) reflectance or Digital Number (DN) in a pixel is a linear summation of the reflectance of each endmember multiplied by the surface fraction it covers; (2) each photon interacts with a single land cover type within the instantaneous field of view, and no scattered photons interact with multiple land cover; (3) adjacent pixels do not affect the spectra of the target pixel.

The mechanism can be described by the following equation:

$$D_{N_i} = \sum_{j=1}^{p} m_{ij}\,\alpha_j + e_i \qquad i = 1,2,\cdots,L;\ j = 1,2,\cdots,p \tag{1}$$

where D_{N_i} is the digital number for each band j in the ETM+ image, L is the number of bands, p is the number of endmembers, m_{ij} is the digital number of endmember j in band j, α_j is the fraction of endmember j, and e_i is the unmodeled residual of band j. By selecting appropriate endmembers, the fraction of each endmember is obtained by applying a least squares technique in order to minimize the unmodeled residual error e_i. Whether the selected endmembers are rational or not is important to the unmixed result.

Ridd (1995) proposed the vegetation, impervious surface, and soil (V-I-S) concept model to characterize the biophysical composition of urban areas. In the model, he considered that urban landscape can be constituted of vegetation, impervious surfaces, and soil. Together with the SMA model, which has a physical meaning and can be understood by non-scientific people, the V-I-S model was used widely in impervious surface extraction; and vegetation, impervious surface, and soil spectra became the most popular endmember spectra that enable decomposition of pixels into fractional components or endmembers. Afterward, a variety of different endmember combinations were developed for the SMA model (Phinn, *et al*., 2002; Rashed, *et al*., 2001, 2003; Wu & Murray, 2003; Wu, 2004; Lu & Weng, 2004; Lu & Weng, 2006a, b). In order to reduce the spectral variability of the same endmember due to their different brightness, some researchers developed the Normalized Spectral Mixture Analysis (NSMA) model (Wu, 2004) and the MESMA model (Roberts, *et al*., 1998b; Dennison & Roberts, 2003; Rashed, *et al*., 2003; Powell, *et al*., 2007).

Considering the strong spectral variability of impervious surfaces and other land covers in the Hai Basin, the MESMA model was

used to estimate the impervious surface coverage. In a traditional MESMA model, the number and type of endmembers vary on a per-pixel basis, and the spectra of each endmember can contain several or dozens of spectra that constitute the spectral library of endmembers. When the MESMA model was applied, the endmember spectra was selected from the spectra library, and many decomposition fractions were obtained. Among all these results, the optimal spectra combination of endmembers was the spectra combination that made the unmodeled residual error minimal. This method for endmember selection can help reduce the unmodeled residual error, but the impervious surface fraction lacks continuity, and the polygons are broken; in addition, the model efficiency is low because the researcher must deal with dozens of satellite images.

In this study, when applying the MESMA model, we selected only two to three spectra for each endmember to represent the spectral variability and to build the spectral library of endmembers. In this way, not only was the unmodeled residual error controlled, but also the decomposition results were continuous and readable.

The specific technical flow of extracting the impervious surface is shown in Fig 1.

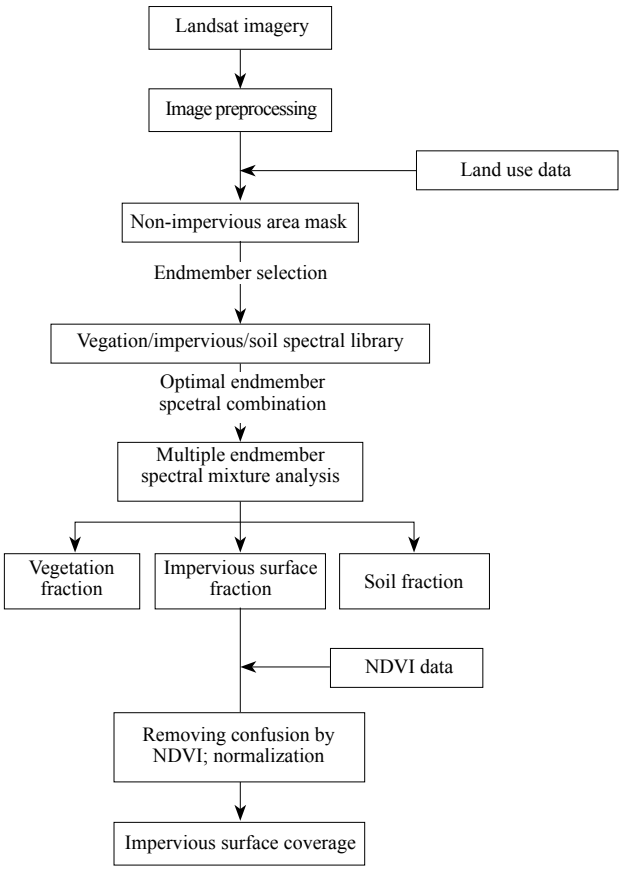

Fig. 1 Flow chart of extracting the impervious surface

2.3 Endmember selection

Endmember selection is the key to success in an SMA model, and we needed to determine the type and spectral number of the endmember. In this study, we selected vegetation, impervious surface, and soil as endmembers for the input of the SMA model, and the model were applied for all images in the study area to extract impervious surface coverage by selecting the appropriate endmember; thus we were able to determine a reliable result in each scene.

Many methods can be used for endmember selection (Lu & Weng, 2004), and we used visual interpretation methods to select image endmembers manually by combining the original Landsat images and SPOT5 high-resolution images of the study area. In this way, a high accuracy result can be obtained (Fan, 2008).

The vegetation endmember, which was bright vegetation and dark vegetation, was selected from farmland and dense forest areas on the mountains; the impervious surface endmember, which included both high albedo and low albedo impervious surfaces, was selected from the center of roads, roofs, and airports; the soil endmember, which was dry and wet soil, was selected from uncultivated farmland and the reservoir bank (Fig. 2).

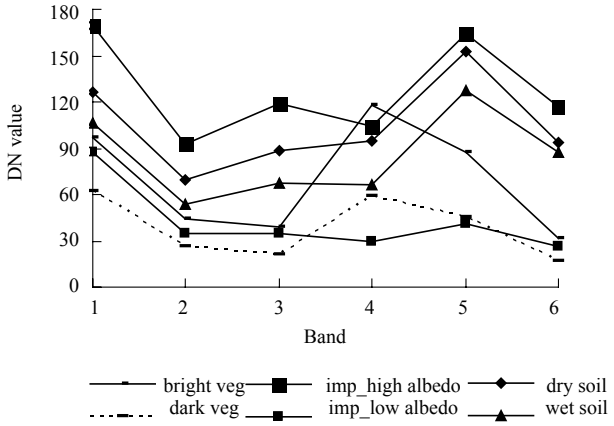

Fig. 2 Different spectral curve of endmembers

Not all types and spectra of endmembers must be selected in each image, and the necessary specific types and spectra depend on the spectral variation of landtypes in each scene. This endmember selection method improves the speed of both endmember selection and model calculation.

2.4 Extraction of impervious surface coverage and post-processing

Based on the different spectral combinations of vegetation, impervious surface, and soil from the endmembers spectral library, we can determine many decomposition results by applying the MESMA model. From these results, we chose the optimal vegetation fraction, impervious surface fraction, and soil fraction when the unmodeled residual error was minimal.

The original impervious fraction—that is, impervious surface coverage—required a series of image processing to remove the irrationality to reach more reality and accuracy. The specific process was as follows:

(1) Removal of confusing vegetation

Impervious surfaces easily can be confused with some vegetation, and this confusion can be removed using NDVI

$$ISC=0 \text{ when } NDVI>NDVI^0 \quad (2)$$

where ISC is impervious surface coverage. $NDVI^0$ is a threshold that separates impervious surfaces from vegetation, and it can be obtained by using an interactive view between impervious surface coverage and original ETM+ images.

(2) Normalization

Influenced by the differences in image acquisition time, atmospheric

conditions, and other factors, the impervious surface coverage from different images, which were determined by applying the MESMA model, cannot be compared with each other, but we can normalize the original imperious surface coverage to make it range from zero to one.

$$\begin{aligned} ISC^* &= \frac{ISC - ISC_{soil}}{ISC_{max} - ISC_{soil}} \cdots ISC \in (ISC_{soil}, ISC_{max}) \\ ISC^* &= 0 \cdots\cdots ISC < ISC_{soil} \\ ISC^* &= 1 \cdots\cdots ISC > ISC_{max} \end{aligned} \quad (3)$$

where ISC^* is the impervious surface coverage after normalization, ISC is the original impervious surface coverage, ISC_{soil} is impervious surface coverage of soil, and ISC_{max} is the impervious surface coverage when a pixel is coverage by pure impervious surface.

3 RESULTS AND ACCURACY ASSESSMENT

After a series of image processing, we obtained the impervious surface coverage of the Hai Basin (Fig. 3). Next, we will introduce the method and result of accuracy assessment of impervious surface coverage.

Classifying the aerial orthophotograph using an unsupervised method, we obtained the impervious surface distribution with a resolution of 1 meter, and the land type in a pixel could be considered pure. We later manually modified the misclassified land types in the ARCMAP using visual interpretation. Then we calculated the proportion of impervious surface type per assessment unit, and the proportion could be deemed as the actual impervious surface coverage due to the lack of ground verification data. Therefore, we could use this data to evaluate the accuracy of the estimated impervious surface coverage.

Most important, in order to evaluate the accuracy of estimated impervious surface coverage, we used the following strategies and principles: (1) we can use an equalized random sampling method in the study area; (2) when we calculate the actual coverage from the orthophotograph, we can choose a 3×3 Landsat pixels window as the assessment unit, which contains 8100 orthophotograph pixels. Therefore, the impervious surface coverage represents an average impervious surface percent in the 8100-square-kilometer units, which can reduce the registration error between the aerial orthophotograph and the Landsat image.

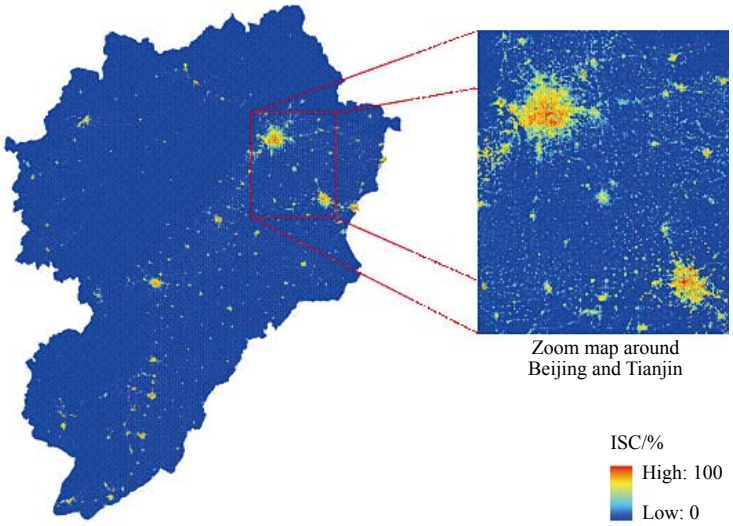

Fig. 3 ISC of Hai Basin

We selected a mean relative error (MRE) and the correlation coefficient (R) between actual impervious surface coverage and estimated impervious surface coverage as the accuracy assessment indices,

$$MRE = \frac{\sum_{i=1}^{n} \left(\left| ISC_{i\,real} - ISC_{i\,assessment} \right| / ISC_{i\,real} \right)}{n} \quad (4)$$

where MRE is mean relative error, $ISC_{i\,real}$ is the actual impervious surface coverage in sample i, $ISC_{i\,assessment}$ is the estimated impervious surface coverage in sample i, and n is the number of samples.

Because the quantity of aerial photographs is limited, we made an accuracy assessment only in some places around the Huairou and Miyun areas. The MRE and R of all samples was 12.1% and 0.83, respectively, which indicated good accuracy. Based on visual comparisons between the estimated impervious surface coverage and the Landsat ETM+ images, the estimated results in other regions were reliable, and the overall accuracy was good. From Fig. 4, we clearly can see that the impervious surface coverage in parks and croplands is lower, impervious surface coverage in buildings is higher, and the distribution of estimated impervious surface coverage corresponds to the actual distribution.

4 CONCLUSION AND DISCUSSION

In this study, by selecting bright and dark vegetation endmember, high albedo and low albedo impervious surface endmember, and dry and wet soil endmember, we applied the MESMA model together with land use data to extract impervious surfaces. With this method, we obtained impervious surface coverage in the Hai Basin in 2000. In the process of extracting impervious surfaces, we took full advantage of the non-impervious information of urban residential land, rural residential land, industrial areas, roads, and rail land use and generated the mask of non-impervious surfaces, which rapidly confine the extent of the impervious surface region. The final impervious surface result contained not only the spatial distribution information but also the coverage information of impervious surfaces.

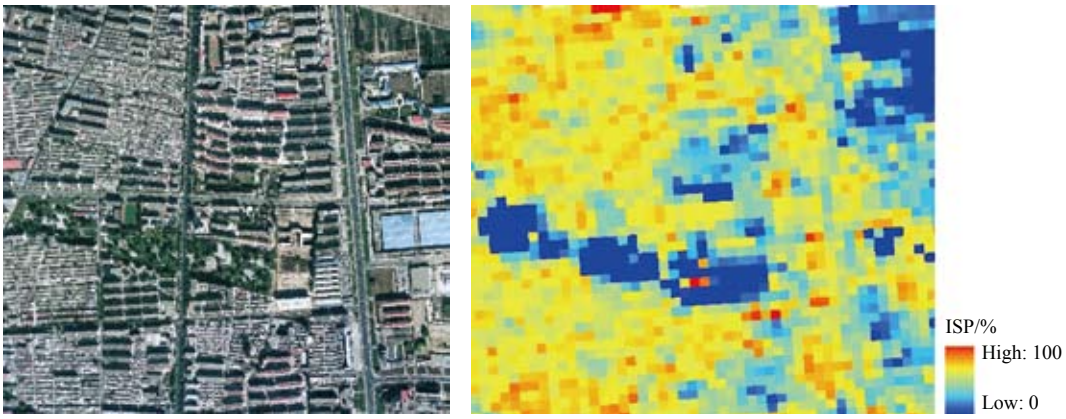

(a) (b)

Fig. 4 Part of the Huairou County aerial photograph and the ETM + estimated impervious surface coverage result
(a) A corner of the Huairou County aerial orthophotograph; (b) Estimated impervious surface coverage

The results of the accuracy assessment showed the validity of the method, which was considered a rapid and exact remote sensing method of extracting impervious surfaces. Because high-resolution data were scarce, we evaluated the estimated impervious surface coverage only in some local areas but not in the entire study area, and to some extent, this does not make the accuracy of impervious surface extraction convincing. Considering that we used the same method and the same image processing techniques to extract impervious surfaces everywhere in the Hai Basin, we believe that the areas where we did not assess accuracy has similar accuracy.

On the one hand, the land use data can avoid confusion between impervious surface and other land types in non-impervious surface areas. For example, soil in uncultivated land may be difficult to distinguish from sand in a dry riverbed, and shadows caused by tall buildings and large tree crowns in urban areas also may be difficult to separate from impervious surfaces, which may lead to underestimation of impervious surface areas. On the other hand, in the process of extracting impervious surfaces, the impervious surface coverage in non-impervious surface areas was deemed as zero, which may ignore the existing impervious surfaces in these areas. Non-impervious area is a relative concept, and the spatial resolution of land use data restricts the discovery of impervious surfaces. For example, farmers use many impervious surfaces for storing water, but we cannot interpreter them from Landsat images. As the image spatial resolution increases, imperious surfaces may be found in former non-impervious surfaces.

To some extent, the MESMA method can solve the problems that different spectra exist in a land type, and a pixel may include many different land types. However, the fact that similar spectra may exist in different land types may lead to a lower accuracy in some areas. For example, the low albedo impervious surface may have similar spectra as water and shadows caused by large tree crowns and tall buildings; the high albedo impervious surface also may share similar spectra as urban bare soil. All of these inevitably may result in the MESMA model residual error.

The spectral similarity of different land types affects the accuracy of estimated impervious surface when applying both the SMA method and other remote sensing-based methods; therefore, we must take appropriate measures to eliminate this effect so as to improve the accuracy of impervious surface extraction. Two possible methods may overcome this problem, as follows.

(1) Combine multispectral images with other auxiliary thematic data

More auxiliary thematic data can provide more useful information and will make distinguishing the confusing land types easier. For example, NDVI data can reduce the confusion between vegetation and impervious surfaces.

In addition, we can use the temperature data generated by infrared band to separate low albedo impervious surfaces from shadows and water (Lu & Weng, 2006). The texture of buildings and surface roughness extracted by radar data also is useful to separate impervious from other land types.

(2) Apply hyperspectral images

That similar spectra exist in different land types is a relative concept. As the bands of a hyperspectral sensor increase, the confused land types in multispectral images would be distinguished easily, which may lead to different spectra in different land types (Weng, *et al*., 2008).

By applying the impervious surface extraction method of remote sensing in a basin scale as proposed in this paper, we have obtained impervious surface coverage distributions in the Hai Basin for the following four periods: 1980, 1990, 2000, and 2007. Next, together with other land surface parameters, such as land use, soil types, and vegetation coverage, we will analyze the spatial and temporal pattern of the land surfaces. Then, combining this data with rainfall, evapotranspiration from hydrometeorological sites, field infiltration, and evapotranspiration data, and other relevant data, we will explore the reasons why the water resource in the Hai Basin changes. Finally, we will assess the water resource over 30 years by using statistical analysis and the distributed hydrological model.

REFERENCES

Arnold C L and Gibbons C J. 1996. Imperious surface coverage: the emergence of a key environmental indicator. *Journal of the American Planning Association*, **62**(2): 243–258

Bauer M E, Heiner N J, Doyle J K and Yuan F. 2004. Impervious surface mapping and change monitoring using Landsat remote sens-

ing. ASPRS Annual Conference Processings, 23–28 May 2004, Denver, Colourado, American Society for Photogrammetry and Remote Sensing, Bethesda, Maryland

Brabec E, Schulte S and Richards P L. 2002. Impervious surfaces and water quality: a review of current literature and its implications for watershed planning. *Journal of Planning Literature*, **16**(4): 499–514

Brun S E and Band L E. 2000. Simulating runoff behavior in an urbanizing watershed. *Computers, Environment and Urban Systems*, **24**(1): 5–22

Civco D L and Hure J D. 1997. Impervious surface mapping for the state of Connecticut. Proceedings of the American Society for Photogrammetry and Remote Sensing Annual Conference. 7–10 April 1997, Seattle, WA, USA (Bethesda, MD: American Society for Photogrammetry and Remote Sensing), 124–135

Dennison P E and Roberts D A. 2003. Endmember selection for multiple endmember spectral mixture analysis using endmember average RMSE. *Remote Sensing of Environment,* **87**(2–3): 123−135

Dougherty M, Dymond R L, Goetz S J, Jantz C A and Goulet N. 2004. Evaluation of impervious surface estimates in a rapidly urbanizing watershed. *Photogrammetric Engineering and Remote Sensing*, **70**(11): 1275–1284

Gillies R R, Box J B, Symanzik J and Rodemaker E J. 2003. Effects of urbanization on the aquatic fauna of the Line Creek watershed, Atlanta—a satellite perspective. *Remote Sensing of Environment*, **86**(3): 411–422

Hodgson M E, Jensen J R, Tullis J A, Riordan K D and Archer C M. 2003. Synergistic use of Lidar and color aerial photography for mapping urban parcel imperviousness. *Photogrammetric Engineering and Remote Sensing*, **69**(9): 973–980

Jennings D B, Jarnagin D B, Jarnagin S T and Ebert C W. 2004. A modeling approach for estimating watershed impervious surface area from national land cover data 92. *Photogrammetric Engineering and Remote Sensing*, **70**(11): 1295–1307

Lu D and Weng Q. 2004. Spectral mixure analysis of the urban landscape in Indianapolis with Landsat ETM+ imagery. *Photogrammetric Engineering and Remote Sensing*, **70**(9): 1053–1062

Lu D and Weng Q. 2006. Use of impervious surface in urban land use classification. *Remote Sensing of Environment*, **102**(1–2): 146–160

Lu D and Weng, Q. 2006. Spectral mixture analysis of ASTER imagery for examining the relationship between thermal features and biophysical descriptors in Indianapolis, Indiana. *Remote Sensing of Environment*, **104**(2): 157–167

Oke T. 1987. Boundary Layer Climates, Routledge, New York

Phinn S, Stanford M, Scarth P, Murray A T and Shyy P T. 2002. Monitoring the composition of urban environments based on the vegetation-impervious surface-soil (VIS) model by subpixel analysis techniques. *International Journal of Remote Sensing*, **23**(20): 4131–4153

Powell R L, Roberts D A, Dennison P E and Hess L L. 2007. Sub-pixel mapping of urban land cover using multiple endmember spectral mixture analysis: Manaus, Brazil, *Remote Sensing of Environment*, **106**(2): 253–267

Rashed T, Weeks J R, Gadalla M S and Hill A.2001. Revealing the Anatomy of Cities through Spectral Mixture Analysis of Multispectral Imagery: A Case Study of the Greater Cairo Region, Egypt. *Geocarto International*, **16**(4): 5–16

Rashed T, Weeks J R, Roberts D, Rogan J and Powell R. 2003. Measuring the physical composition of urban morphology using multiple endmember spectral mixture models. *Photogrammetric Engineering and Remote Sensing*, **69**(9): 1011–1020

Ridd M K. 1995. Exploring a V-I-S (Vegetation-Impervious Surface-Soil) model for urban ecosystem analysis through remote sensing: comparative anatomy for cities. *International Journal of Remote Sensing*, **16**(12): 2165–2185

Roberts D A, Gardner M, Church R, Ustin S, Scheer G and Green R O. 1998b. Mapping chaparral in the Santa Monica mountains using multiple endmember spectral mixture models. *Remote Sensing of Environment*, **65**(3): 267–279

Schueler T R. 1994. The importance of imperviousness. *Watershed Protection Techniques*, **1**(3): 100–111

Weng Q. 2001. Modeling urban growth effect on surface runoff with the integration of remote sensing and GIS. *Environmental Management*, **28**(6): 737–748

Weng Q and Lu D. 2008. A sub-pixel analysis of urbanization effect on land surface temperature and its interplay with impervious surface and vegetation coverage in Indianapolis, United States. *International Journal of Applied Earth Observation and Geoinformation*, **10**(1): 68–83

Wu C. 2004. Normalized spectral mixture analysis for monitoring urban composition using ETM+ imagery. *Remote Sensing of Environment*, **93**(4): 480–492

Wu C and Murray A T. 2003. Estimating impervious surface distribution by spectral mixture analysis. *Remote Sensing of Environment*, **84**(10): 493–505

Xian G. 2007. Analysis of impacts of urban land use and land cover on air quality in the Las Vegas region using remote sensing information and ground observations. *International Journal of Remote Sensing*, **28**(24): 5427–5445

Yang L, Huang C, Homer C G, Wylie B K and Coan M J. 2003a. An approach for mapping large-scale impervious surfaces: synergistic use of Landsat-7 ETM+ and high spatial resolution imagery. *Canadian Journal of Remote Sensing*, **29**(2): 230–240

Yang L, Xian G, Klaver J M and Deal B. 2003b. Urban land cover change detection through sub-pixel imperviousness mapping using remotely sensed data. *Photogrammetric Engineering and Remote Sensing*, **69**(9): 1003–1010

Yang X. 2006. Estimating landscape imperviousness index from satellite imagery. *IEEE Geoscience and Remote Sensing Letters,* **3**(1): 6–9

Yuan F and Bauer M E. 2006. Comparison of impervious surface area and normalized difference vegetation index as indicators of surface urban heat island effects in Landsat imagery. *Remote Sensing of Environment*, **106**(3): 375–386

Zug M, Phan L, Bellefleur D and Scrivener O. 1999. Pollution wash-off modeling on impervious surface: calibration, validation and transposition. *Water Science and Technology*, **39**(2): 17–24

流域尺度的不透水面遥感提取

王浩，吴炳方，李晓松，卢善龙

中国科学院 遥感应用研究所，北京 100101

摘 要：一个地区的不透水面覆盖度不仅是该地区城镇化程度重要指示因子，也是该地区生态环境状况的重要指示因子。现有的不透水面遥感提取方法，多集中在城区尺度上。而流域尺度上快速、准确的不透水面遥感提取方法在国内外还鲜有研究。本研究以覆盖海河流域同一季节的Landsat影像为数据源，利用已有土地利用数据集中的道路、城市、农村和工业用地对非不透水区进行掩膜，通过选取亮暗植被、高低反照度不透水面、干湿土壤端元，采用多端元光谱混合分解模型提取了流域尺度上的不透水面。精度评价结果显示，该方法估算的不透水面与真实结果之间的平均相对误差为12.1%，相关系数为0.83，精度较高，适合于流域尺度的不透水面提取。

关键词：不透水面，流域尺度光谱混合分解，遥感，海河流域

中图分类号：TP75/TP79 **文献标志码**：A

引用格式：王浩，吴炳方，李晓松，卢善龙. 2011. 流域尺度的不透水面遥感提取. 遥感学报，**15**(2): 388–400
Wang H, Wu B F, Li X S and Lu S L. 2011. Extraction of impervious surface in Hai Basin using remote sensing. *Journal of Remote Sensing*, **15**(2): 388–400

1 引 言

不透水面定义为诸如屋顶、沥青或水泥道路以及停车场等具有不透水性的地表面（Arnold和Gibbons，1996）。不透水面盖度为某一区域内不透水面覆盖面积所占整个区域面积的比例。随着社会经济的发展，中国城镇化水平越来越高。城镇化的快速发展导致了地表不透水面的增加。

在城区尺度上，不透水面盖度是城镇化程度的重要指示器，现已广泛用于居民区的人口估算（Wu和Murray，2005；Lu 等，2006），土地利用/土地覆盖制图（Madhavan 等，2001；Phinn 等，2002；Lu和Weng，2006；Pu 等，2008），城市土地利用规划（Brabec 等，2002）。此外，不透水面吸收大量的短波太阳辐射，而后又以长波辐射的形式发射出去加热城市冠层和边界层，改变其显热和潜热通量（Oke，1987；Yuan和Bauer 2006），从而影响城市气候，甚至对城市群气候产生影响。

不透水面还是流域水文循环和水资源评价中的重要下垫面特征。在流域尺度上，降水在不透水面地区难以入渗到土壤，从而减少了对土壤水和地下水的补给；相反，降水更多的以地表径流的方式汇入河网，使得地表径流增加，同时也增加了暴雨来临时的洪水发生频率（Weng，2001；Brun和Band，2000）。此外，不透水面和径流的增加直接影响包括病原体、营养物、有毒物和沉淀物在内的非点源污染物传播（Hurd和Civco，2004），从而不可避免的对水质和水生环境产生极为负面的影响（Zug 等，1999；Brabec 等，2002；Gillies 等，2003）。通常情况下，当一个流域的不透水面盖度超过10%，河流的健康状况就会下降（Schueler，1994）。

不透水面的遥感提取方法主要有基于像元的分类方法（Hodgson 等，2003；Dougherty 等，2004；Jennings 等，2004）和亚像元提取方法（Gillies 等，2003；Bauer 等，2004；Yang，2006；Murray，2003；Wu 等，2004；Lu和Weng，2006；Civco

收稿日期：2010-06-02；**修订日期**：2010-08-02

基金项目：中国科学院知识创新重大工程（编号：KZCX1-YW-08-03）；国家科技支撑计划（编号：2006BAJ11B09）。

第一作者简介：王浩（1985— ），男，河北唐县人，中国科学院遥感应用研究所博士研究生，目前主要从事流域下垫面要素反演，水资源量遥感估算等方面研究。E-mail: wanghao@irsa.ac.cn。

通信作者：吴炳方，E-mail: wubf@irsa.ac.cn。

和Hurd，1997；Yang 等，2003a，b；Jantz 等，2005；Xian，2007）。在传统的不透水面提取中，基于像元的分类方法长期占据主导地位，在该方法中不透水面被视为一种地类，通过各种监督、非监督分类可以得到。由于受限于影像的空间分辨率，不透水面与其他地类的混合问题非常突出。为了解决混合像元问题，亚像元水平的不透水面遥感提取得到了发展，提取方法包括多元回归模型（Gillies 等，2003；Bauer 等，2004；Yang，2006）、光谱混合分解（Wu和Murray，2003；Wu 等，2004；Lu和Weng，2006）、人工神经网络（Civco和Hurd，1997）、分类回归树（Yang，2003a，b；Jantz 等，2005；Xian，2007）等。亚像元水平的不透水面遥感提取，使得原来像元中单一的地物类型表达被连续的不透水面盖度所取代，不透水面的提取由此进入到定量化水平的阶段。

虽然国内外学者已经做了大量的不透水面提取方法的研究，但是几乎所有的研究都限定在城区尺度上，缺乏一种在流域尺度上快速准确的不透水面提取方法。具有闭合性的流域是水循环研究中的最基本单元，水资源开发利用、河道治理规划、水循环过程研究等都是在流域尺度上进行的。因此，通过遥感方法提取整个流域的不透水面分布，对于水循环研究和水资源评价有着重要的意义。

本文旨在探究一种流域尺度上的不透水面遥感提取方法，绘制全流域的不透水面分布图，从而为流域的水循环研究提供服务。以海河流域为研究区，采用Landsat ETM+卫星影像和辅助土地利用数据相结合的方法，通过手工选取多个亮暗植被端元、高低反照度不透水面端元、干湿裸土端元，应用多端元的光谱混合分解模型快速提取不透水面盖度，并通过NDVI阈值选取、初始不透水面归一化等技术得到全海河流域准确的不透水面分布。

2 数据和方法

2.1 数据及预处理

2.1.1 Landsat ETM+数据

覆盖海河流域的2000期Landsat影像共20景，获取时间为1999年7月1日至2002年5月22日，各景影像的拍摄时间均处在春末至秋初的植被生长期。影像数据由USGS网站上下载，下载的影像本身已经进行了几何纠正，所以没有重新对其进行几何校正。各景影像均为无云或极少云，质量较高，也未对其进行大气校正。

2.1.2 土地利用数据

研究中使用的土地利用数据为中国科学院资环局利用同一ETM+影像数据集制作的2000年土地利用数据集，由于不透水面提取过程中关注的重点是城镇化地区的不透水面，故排除了农田区及林草地等不透水面较少的地区。

将土地利用数据集中的城镇居民用地（代码：71）、乡村居民用地（代码：72）、工矿用地（代码：61）、公路（代码：101）、铁路（代码：102）地类合并，生成不透水面掩膜区，去除其他地类，从而提高不透水面盖度的提取精度和准确度。

2.1.3 高分辨率影像数据

高分辨率影像为航空飞机拍摄的航片，拍摄时间为2000年8月，空间分辨率为1 m，用来检验不透水面提取结果的精度，由于其空间分辨率较高，经土地利用分类得到的不透水面可当作真实不透水面，因此它能够对不透水面的遥感提取结果进行精度评价。

2.2 模型的确定

线性光谱混合模型定义为像元在某一波段的反射率是由有限个不同端元的反射率以其所占像元面积比例为权重系数的线性组合（赵英时，2003），它基于以下三点假设：（1）像元在某一波段的反射率（亮度值）是由构成像元的端元的反射率以其所占像元面积比例为权重系数的线性组合；（2）瞬时视场内的端元是同质地、相互隔离的，不存在端元间的多重散射；（3）相邻像元对目标像元的光谱没有影响。

其机理可以由下式描述：

$$D_{N_i} = \sum_{j=1}^{p} m_{ij}\,\alpha_j + e_i \qquad i = 1,2,\cdots,L;\ j = 1,2,\cdots,p \tag{1}$$

式（1）中D_{N_i}为像元在第i个波段的灰度值；L为光谱波段数；p为像元内端元数；m_{ij}表示像元内第j端元在第i波段的灰度值；α_j为像元内第j端元所占的面积比例；e_i为第i波段灰度值误差项。通过选取合适的端元的光谱信息，并结合混合像元的光谱值即可反求出各个端元的组分比例，端元的合理选择与否，对最终分解结果有着重要的影响。

Ridd（1995）提出了表征城市生物物理组成的V-I-S（Vegetation- Impervious Surface- Soil）模型，

该模型认为城市景观可由植被、不透水面和裸土3种组分构成。V-I-S概念模型与具有明确物理意义的线性光谱混合分解模型（Spectral Mixture Analysis，SMA）相结合广泛用于城市地区不透水面的亚像元提取，植被、不透水面及裸土也成为影像像元光谱混合分解中常采用的端元。随后，用于光谱混合分解模型中的其他端元组合得到了发展（Phinn 等，2002；Rashed 等，2001，2003；Wu和Murray，2003；Wu，2004；Lu和Weng，2004；Lu和Weng，2006a，b）。为了减少同类地物由于亮度差异而产生的光谱变异，又有学者发展了端元亮度归一化的光谱混合分解模型（Wu，2004）和多端元的光谱混合分解模型（Roberts 等，1998b；Dennison和Roberts，2003；Rashed 等，2003；Powell 等，2007）。

海河流域内不透水面及其他端元的光谱空间变异性很强，可采取多端元的光谱分解模型对不透水面盖度进行估算。传统的多端元光谱分解模型中，模型分解使用的端元种类可以变化，每种端元的光谱数目也可以变化。通常情况下，对模型使用的各端元分别选取几个或几十个光谱构成该端元的光谱库；每个像元分解时，各端元均从光谱库中选取一种光谱，从而得到多种分解结果；根据模型分解得到的残差选取残差最小残差所对应的分解结果作为像元的最终结果。端元的这种选择策略虽然能减少模型分解所产生的误差，但分解得到的不透水面盖度结果缺少连续性，图斑非常破碎，而且对于几十景的影像，解算起来运行效率非常低。

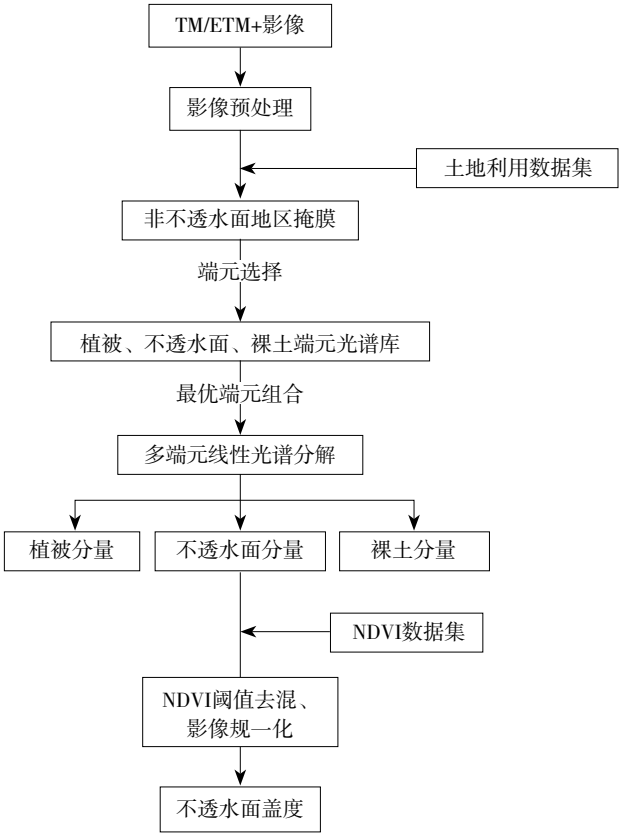

图1 不透水面提取流程图

本研究采用的多端元光谱分解模型对每种端元类型仅选择2到3种具有代表性的光谱构成端元光谱库，对每个像元进行多端元的光谱混合分解，这种端元的选取策略不仅能从宏观上控制模型的误差，又能使结果具有很好的连续性和可读性。

具体技术路线如图1所示。

2.3 端元选取

端元的选取是模型成功与否的关键，端元的种类和数目均需确定。本研究选取植被、不透水面、裸土这三种端元作为线性光谱分解模型的输入。研究区内所有的影像通过选取合适的影像端元来确保每景影像分解得到的不透水面盖度可靠。

端元的选取有很多种方法（Lu和Weng，2004），本研究将原始影像和已有的SPOT5高分辨率影像相结合，采用目视解译的方法在影像上手工选取端元。这主要是因为通过目视的方法手工选取影像端元，可以取得很高的分解精度（樊风雷，2008）。

植被端元从农田和山地林木密集区选取，分为亮植被和暗植被；不透水面端元从道路中央、屋顶和机场处选取，分为高反照度不透水面、低反照度不透水面；裸土从修耕的农田中或水库的两岸空地处选取，分为干裸土和湿裸土（图2）。

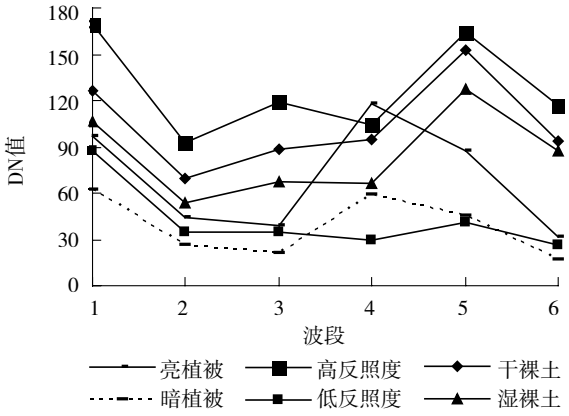

图2 同一端元类型的不同光谱曲线图

并非每景影像必须选取上述各端元光谱，需要选取的端元类型和光谱视影像中地物的光谱变异性而定。这种多端元的选取方法，不仅提高了端元选取的

速度，也加快了模型的运行速度。

2.4 不透水面盖度估算及后处理

根据每景影像所选取的植被、不透水面、裸土端元中的不同光谱组合，进行光谱混合分解，从而得到不同的分解结果。从多个结果中选取模型分解残差最小的植被分量、不透水面分量和裸土分量。

初始得到的不透水面分量，即不透水面盖度，需经过一系列操作处理，消除不合理之处，得到更加符合实际的不透水面盖度。具体处理如下：

（1）混淆植被去除

一些植被容易同低覆盖度的不透水面混淆，通过NDVI予以去除

$$ISC=0 \text{ 当} NDVI>NDVI^0 \quad (2)$$

ISC为不透水面盖度，$NDVI^0$为低覆盖度的不透水面与植被混淆的一个临界NDVI值，通过在初始不透水面盖度结果图和原始ETM+影像图中交互浏览获得。

（2）归一化处理

由于影像的获取时间、大气状况等因素的影响，每景影像分解后获得的不透水面盖度值缺乏可比性，因此采用归一化的方法将其转化到0到1范围内。

$$\begin{aligned} ISC^* &= \frac{ISC - ISC_{soil}}{ISC_{max} - ISC_{soil}} \cdots ISC \in (ISC_{soil}, ISC_{max}) \\ ISC^* &= 0 \cdots\cdots\cdots\cdots\cdots\cdots ISC < ISC_{soil} \\ ISC^* &= 1 \cdots\cdots\cdots\cdots\cdots\cdots ISC > ISC_{max} \end{aligned} \quad (3)$$

式中ISC^*为归一化处理后的不透水面盖度值；ISC为原始不透水面盖度值；ISC_{soil}为裸土的不透水面盖度值；ISC_{max}为地表完全为不透水面时盖度值。

3 结果与精度评价

经过一系列处理后得到了海河流域的不透水面盖度图（图3）。接下来，将对不透水面盖度的精度评价方法和评价结果进行介绍。

首先，对1 m空间分辨率的航空正射影像进行分类，获得包含不透水面在内的分类结果，结果中每个像元可以认为是纯像元，不存在地类的混合现象；然后，在Arcmap中目视解译手工修改不合理的不透水面分类结果，获得不透水面分布。计算精度评价单元内不透水面面积所占的比例，由于缺乏野外实地验证数据，该比例可假定为单元内真实的不透水面盖度值，所以可用于对估算的不透水面盖度进行精度评价。

为了对估算结果进行合理评价，尤其应考虑以下几个原则：

（1）在研究区内通过分层随机采样的方法选择精度验证样本的位置；（2）当从航空相片中计算真实不透水面盖度时，每个样本点选取3 × 3（90 m × 90 m）的像元窗口作为精度评价单元，以减小影像配准误差对精度评价的影响，即一个样本点对应3 × 3=9个ETM+像元，8100个航空正射影像像元；通过聚类的方法获取90 m × 90 m评价单元下航片的真实不透水面盖度和ETM+估算的不透水面盖度估算结果。

选取不透水面盖度真实值与不透水面估算值两者的平均相对误差（MRE）和相关系数（R）作为不透水面盖度的精度评价标准：

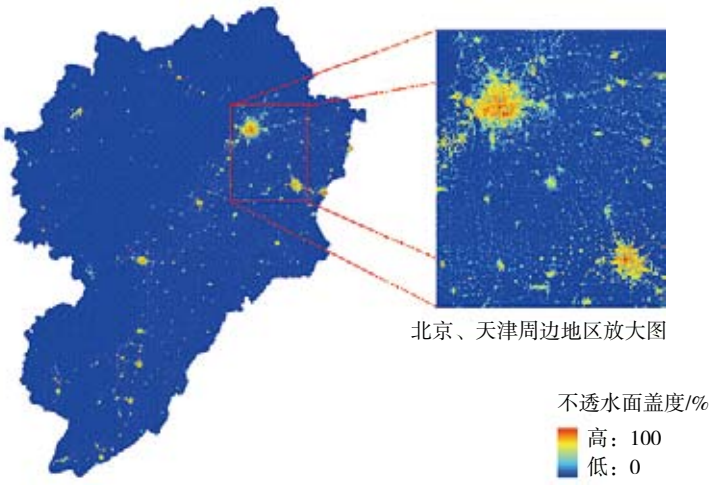

图3 海河流域不透水面盖度分布

$$\mathrm{MRE}=\frac{\sum_{i=1}^{n}\left(\left|\mathrm{ISC}_{i\text{真实}}-\mathrm{ISC}_{i\text{估算}}\right|/\mathrm{ISC}_{i\text{真实}}\right)}{n} \quad (4)$$

式中MRE为平均相对误差；$\mathrm{ISC}_{i\text{真实}}$为第$i$个样本处不透水面盖度真实值；$\mathrm{ISC}_{i\text{估算}}$为第$i$个样本处不透水面盖度估算值；$n$为样本的个数。

由于航片数量有限，仅对怀柔、密云地区及周围的不透水面盖度进行了精度评价，所有样本计算求得的平均相对误差MRE和相关系数R分别为12.1%和0.83，由此可知不透水面盖度的提取具有较好的精度。其他地区通过原始影像与最终的不透水面盖度结果目视比较的方式进行精度评价，结果发现估算结果真实可信，不透水面盖度结果进行总体精度较高。从图4中可以清楚的看到，公园和城市边上的农田地区不透水面盖度较低，而在建筑群地区不透水面盖度较高，不透水面盖度分布与实际相符。

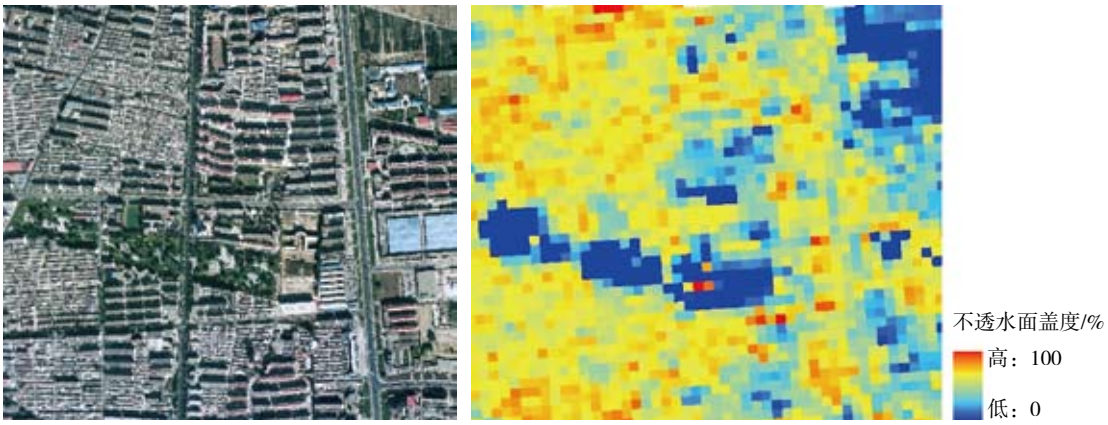

（a） （b）

图4 怀柔县城部分地区航片和ETM+估算的不透水面盖度结果

（a）怀柔县城航片一角；（b）不透水面盖度估算结果

4 结论及讨论

本研究通过选取亮、暗植被端元，高、低反照度不透水面端元，干、湿裸土端元，辅以土地利用数据，采用多端元的光谱混合分解模型对流域尺度的不透水面进行了提取，得到了2000年海河流域地区的不透水面盖度图。在不透水面提取过程中，充分利用城镇居民用地、乡村居民用地、工矿用地、公路、铁路等土地利用包含的不透水面信息，生成非不透水区掩膜区，快速准确的界定不透水面区域。最终的不透水面结果，既包含了不透水面的空间分布信息，又包含不透水面的盖度信息。

通过精度验证可知，该方法有效可靠，不失为一种流域尺度上快速准确提取不透水面的遥感方法。由于高分辨率数据较为缺乏，仅对部分地区的不透水面盖度结果进行了精度验证，使该方法获得的结果在一定程度上缺乏说服力，但考虑整个海河流域内不透水面提取均采用相同的方法及操作，由此推断在其他未进行精度验证的地区也有类似的精度。

一方面，海河流域土地利用数据集的使用，有效地避免了非不透水面地区不透水面与其他地物的混淆，如农田内土壤和干河床沙地与不透水面很难区分，山区树冠和地形起伏产生的阴影与不透水面也很易混淆，在这些地区不透水面极易被错误提取而导致不透水面盖度被夸大；另一方面，在不透水面提取过程中，非不透水区的不透水面盖度视为零，忽视了这些地区可能存在的不透水面。而且非不透水区是一个相对概念，区域内的不透水面受土地利用数据源空间分辨率的限制而未被发现。如海河山区有许多农民自挖的储水坑等不透水面，但是在Landsat制作的土地利用中并不能被解译出来。随着影像空间分辨率的提高，原来不透水面地区可能会发现不透水面。

多端元光谱混合分解方法在一定程度上解决了“同物异谱”和“混合像元”问题，但在一些地区由于“异物同谱”，模型分解精度仍不高。树冠和高大建筑产生的阴影以及水体与低反照度的不透水面光谱极为相似，城区裸露空地与高反照度不透水面光谱也极为相似，光谱的相似性必然导致模型分解产生误差。

不同地类的光谱相似性不仅能够对光谱混合分解提取的不透水面精度产生影响，对其他基于遥感方法提取的不透水面精度也存在影响，因此需要采取合适的方法消除这种影响从而提高不透水面的提取精度，以下两种方法使不透水面提取精度的提高成为可能：

方法1　采用多光谱影像结合其他多源辅助专题数据。增加辅助数据集可以获得更多有用信息，区分易混淆地物。NDVI数据集可以减少植被和不透水面的混淆。根据裸土和高反照度不透水面以及区分阴影、水体与低反照度不透水面的温度差异，可以增加热红外波段提取的温度数据集进而将其加以区分（Lu和Weng，2006）。雷达数据提取的人工建筑物等纹理信息和粗糙度信息也有助于不透水面同其他地物的区分。

方法2　高光谱数据的应用。“异物同谱”只是一个相对概念，随着高光谱传感器光谱波段的增加，原来在多光谱影像上混淆的地物可能会出现“异物不同谱”，致使不透水面与其他地物可能在某些波段上很容易区分开（Weng 等，2008）。

目前，通过流域尺度不透水面遥感提取方法已经得到海河流域1980年、1990年、2000年、2007年4期的不透水面盖度分布，下一步将结合其他的下垫面要素，如土地利用、土壤类型、植被覆盖等对海河流域的下垫面时空格局进行分析，结合气象水文站点的降雨、蒸发等数据，野外实测下渗、蒸发等数据以及其他相关数据，采用统计分析和分布式水文模型的方法，探讨30多年来海河流域水资源变化的原因并对水资源进行评价。

REFERENCES

Arnold C L and Gibbons C J. 1996. Imperious surface coverage: the emergence of a key environmental indicator. *Journal of the American Planning Association*, **62**(2): 243–258

Bauer M E, Heiner N J, Doyle J K and Yuan F. 2004. Impervious surface mapping and change monitoring using Landsat remote sensing. ASPRS Annual Conference Processings,23–28 May 2004, Denver, Colourado, American Society for Photogrammetry and Remote Sensing, Bethesda, Maryland

Brabec E, Schulte S and Richards P L. 2002. Impervious surfaces and water quality: a review of current literature and its implications for watershed planning. *Journal of Planning Literature*, **16**(4): 499–514

Brun S E and Band L E. 2000. Simulating runoff behavior in an urbanizing watershed. *Computers*, *Environment and Urban Systems*, **24**(1): 5–22

Civco D L and Hure J D. 1997. Impervious surface mapping for the state of Connecticut. Proceedings of the American Society for Photogrammetry and Remote Sensing Annual Conference. 7–10 April 1997, Seattle, WA, USA (Bethesda, MD: American Society for Photogrammetry and Remote Sensing), 124–135

Dennison P E and Roberts D A. 2003. Endmember selection for multiple endmember spectral mixture analysis using endmember average RMSE. *Remote Sensing of Environment*, **87**(2–3): 123−135

Dougherty M, Dymond R L, Goetz S J, Jantz C A and Goulet N. 2004. Evaluation of impervious surface estimates in a rapidly urbanizing watershed. *Photogrammetric Engineering and Remote Sensing*, **70**(11): 1275–1284

Gillies R R, Box J B, Symanzik J and Rodemaker E J. 2003. Effects of urbanization on the aquatic fauna of the Line Creek watershed, Atlanta—a satellite perspective. *Remote Sensing of Environment*, **86**(3): 411–422

Hodgson M E, Jensen J R, Tullis J A, Riordan K D and Archer C M. 2003. Synergistic use of Lidar and color aerial photography for mapping urban parcel imperviousness. *Photogrammetric Engineering and Remote Sensing*, **69**(9): 973–980

Jennings D B, Jarnagin D B, Jarnagin S T and Ebert C W. 2004. A modeling approach for estimating watershed impervious surface area from national land cover data 92. *Photogrammetric Engineering and Remote Sensing*, **70**(11): 1295–1307

Lu D and Weng Q. 2004. Spectral mixure analysis of the urban landscape in Indianapolis with Landsat ETM+ imagery. *Photogrammetric Engineering and Remote Sensing*, **70**(9): 1053–1062

Lu D and Weng Q. 2006. Use of impervious surface in urban land use classification. *Remote Sensing of Environment*, **102**(1–2): 146–160

Lu D and Weng, Q. 2006. Spectral mixture analysis of ASTER imagery for examining the relationship between thermal features and biophysical descriptors in Indianapolis, Indiana. *Remote Sensing of Environment*, **104**(2): 157–167

Oke T. 1987. Boundary Layer Climates, Routledge, New York

Phinn S, Stanford M, Scarth P, Murray A T and Shyy P T. 2002. Monitoring the composition of urban environments based on the vegetation-impervious surface-soil (VIS) model by subpixel analysis techniques. *International Journal of Remote Sensing*, **23**(20): 4131–4153

Powell R L, Roberts D A, Dennison P E and Hess L L. 2007. Sub–pixel mapping of urban land cover using multiple endmember spectral mixture analysis: Manaus, Brazil, *Remote Sensing of Environment*, **106**(2): 253–267

Rashed T, Weeks J R, Gadalla M S and Hill A.2001. Revealing the Anatomy of Cities through Spectral Mixture Analysis of Multispectral Imagery: A Case Study of the Greater Cairo Region, Egypt. *Geocarto International*, **16**(4): 5–16

Rashed T, Weeks J R, Roberts D, Rogan J and Powell R. 2003. Measuring the physical composition of urban morphology using multiple endmember spectral mixture models. *Photogrammetric Engineering and Remote Sensing*, **69**(9): 1011–1020

Ridd M K. 1995. Exploring a V-I-S (Vegetation-Impervious Surface-Soil) model for urban ecosystem analysis through remote sensing: comparative anatomy for cities. *International Journal of Remote Sensing*, **16**(12): 2165–2185

Roberts D A, Gardner M, Church R, Ustin S, Scheer G and Green R O. 1998b. Mapping chaparral in the Santa Monica mountains using multiple endmember spectral mixture models. *Remote Sensing of Environment*, **65**(3): 267–279

Schueler T R. 1994. The importance of imperviousness. *Watershed Protection Techniques*, **1**(3): 100–111

Weng Q. 2001. Modeling urban growth effect on surface runoff with the integration of remote sensing and GIS. *Environmental Management*, **28**(6): 737–748

Weng Q and Lu D. 2008. A sub–pixel analysis of urbanization effect on land surface temperature and its interplay with impervious surface and vegetation coverage in Indianapolis, United States. *International Journal of Applied Earth Observation and Geoinformation*, **10**(1): 68–83

Wu C. 2004. Normalized spectral mixture analysis for monitoring urban composition using ETM+ imagery. *Remote Sensing of Environment*, **93**(4): 480–492

Wu C and Murray A T. 2003. Estimating impervious surface distribution by spectral mixture analysis. *Remote Sensing of Environment*, **84**(10): 493–505

Xian G. 2007. Analysis of impacts of urban land use and land cover on air quality in the Las Vegas region using remote sensing information and ground observations. *International Journal of Remote Sensing*, **28**(24): 5427–5445

Yang L, Huang C, Homer C G, Wylie B K and Coan M J. 2003a. An approach for mapping large–scale impervious surfaces: synergistic use of Landsat–7 ETM+ and high spatial resolution imagery. *Canadian Journal of Remote Sensing*, **29**(2): 230–240

Yang L, Xian G, Klaver J M and Deal B. 2003b. Urban land cover change detection through sub–pixel imperviousness mapping using remotely sensed data. *Photogrammetric Engineering and Remote Sensing*, **69**(9): 1003–1010

Yang X. 2006. Estimating landscape imperviousness index from satellite imagery. *IEEE Geoscience and Remote Sensing Letters*, **3**(1): 6–9

Yuan F and Bauer M E. 2006. Comparison of impervious surface area and normalized difference vegetation index as indicators of surface urban heat island effects in Landsat imagery. *Remote Sensing of Environment*, **106**(3): 375–386

Zug M, Phan L, Bellefleur D and Scrivener O. 1999. Pollution wash–off modeling on impervious surface: calibration, validation and transposition. *Water Science and Technology*, **39**(2): 17–24

附中文参考文献

樊风雷. 2008. 基于线性光谱混合模型（LSMM）的两种不同端元值选取方法应用与评价—以广州市为例. 遥感技术与应用，**23**(3): 272–277

赵英时. 2003. 遥感应用分析原理与方法. 北京：科学出版社